Computer Aided Geometric Design 80 (2020) 101881

Contents lists available at ScienceDirect

Computer Aided Geometric Design

www.elsevier.com/locate/cagd

Isogeometric shape optimization of an acoustic horn using the teaching-learning-based optimization (TLBO) algorithm

Vinay K. Ummidivarapu [a], Hari K. Voruganti [a,*], Tahsin Khajah [b], Stéphane Pierre Alain Bordas [c,d]

[a] Computational Research Laboratory, Department of Mechanical Engineering, National Institute of Technology Warangal, 506004, India
[b] Department of Mechanical Engineering, University of Texas at Tyler, USA
[c] Institute of Computational Engineering, University of Luxembourg, Luxembourg
[d] Department of Medical Research, China Medical University Hospital, China Medical University, Taichung, Taiwan

ARTICLE INFO

Article history:
Received 11 July 2019
Received in revised form 14 April 2020
Accepted 4 May 2020
Available online 13 May 2020

Keywords:
Shape optimization
Isogeometric analysis (IGA)
TLBO algorithm
Acoustic horn
Multi-frequency

ABSTRACT

Isogeometric shape optimization has been receiving great attention due to its advantages of exact geometry representation and smooth representation of the boundaries. In the present study, the optimum shape of a horn speaker was found to minimize the back reflection and improve impedance matching. The acoustic field was estimated by isogeometric analysis (IGA). Horn reflections are sensitive to the boundary shape and the smooth and non-faceted boundary representation in IGA makes it an attractive platform for shape optimization of acoustic devices. Teaching-Learning-Based Optimization (TLBO) algorithm was used to minimize, the reflection coefficient R, by changing the shape of the horn. The NURBS control points defining the design boundary of the horn were selected as the optimization design variables. Both single and multi-frequency optimization were performed. The objective function values found were considerably lower than those reported in the literature. The three-frequency shape optimization was performed successfully for which no results were reported in the literature due to the convergence issues. From the results, it was shown that the proposed method outperforms previous studies by finding the best shape for the horn that results in minimizing the reflection and produce improved reflection spectra.

1. Introduction

Shape optimization is an interesting and challenging subject in engineering design since it involves performing both analysis and optimization simultaneously. The boundary representation of the domain under consideration affects the shape optimization results as the shape optimization depends only on the boundary changes. Previously, finite element analysis (FEA) was used to perform analyses required for shape optimization which led to drawbacks such as approximated geometry and the occurrence of irregular wiggly optimal shapes. To avoid these wiggly shapes, extra operations such as "filtering method", "parameterization-free method" or so-called "traction method" were used (Bletzinger et al., 2010; Firl et al., 2013; Le et al., 2011; Azegami and Takeuchi, 2006). These drawbacks are due to the use of different basis functions for geometric modeling and analysis and the use of nodes as design variables (Wall et al., 2008). The employed optimization

* Corresponding author.
E-mail address: harikumar@nitw.ac.in (H.K. Voruganti).

https://doi.org/10.1016/j.cagd.2020.101881
0167-8396/

algorithm also has a considerable impact on shape optimization results. The gradient-based optimization algorithms require the computation of complex gradients and suffer from local minima trapping (Farhadinia, 2012).

Isogeometric analysis (IGA) is an alternative computational analysis technique in which the same basis functions used for geometric modeling are used to approximate the field variables (Hughes et al., 2005). With the success of IGA as an alternative analysis technique, shape optimization using IGA has been applied for various applications. Wall et al. (2008) performed preliminary studies on isogeometric structural shape optimization. The locations of control points which were used to define the CAD model were adopted as design variables during the optimization process yielding promising optimal results. Qian (2010) computed full analytical sensitivities to enable the gradient-based isogeometric shape optimization. Nagy et al. (2010) studied structural sizing and shape optimization using IGA by considering the spatial location of the control points and their corresponding weights as design variables. Qian and Sigmund (2011) performed isogeometric shape optimization of topologically complex photonic crystals. Wang et al. (2019b) coupled the extended isogeometric analysis (XIGA) with chaotic particle swarm optimization algorithm (CPSO) to perform shape optimization of the structures with cutouts. Isogeometric shape optimization has been applied to shell structures. Kiendl et al. (2014) performed isogeometric shape optimization of shells using semi-analytical sensitivity analysis and sensitivity weighting. Kang and Youn (2016) performed isogeometric shape optimization of trimmed shells with topologically complex structures. More applications on isogeometric shape optimization of shell structures can be found in Bandara and Cirak (2018) and Hirschler et al. (2019).

The usage of control points as design variables leads to some issues like discretization dependency similar to mesh dependency in FEA-based shape optimization. To address the issues of the discretization-dependency of isogeometric shape optimization, Wang et al. (2017) proposed normalization approaches. The discretization-independency of the proposed approaches was verified on various mechanical and thermal problems. Ha et al. (2010) performed T-spline-based isogeometric shape optimization. The usage of T-splines reduced the number of degrees of freedom while yielding the same optimum design shape. Isogeometric shape optimization was applied to find the optimum shapes for fluid and potential flows, heat conduction (Herath et al., 2015; Gillebaart and De Breuker, 2016; Nørtoft and Gravesen, 2013; Yoon et al., 2013), vibrating structures (Nagy et al. 2011 and Manh et al. 2011), electromagnetic scattering (Nguyen et al., 2012), functionally graded structures (Taheri and Hassani 2014 and Wang et al. 2019a) and other applications described in Ummidivarapu and Voruganti (2017), Wang et al. (2018a), Choi and Cho (2018), Benzaken et al. (2017).

IGA was also coupled with the Boundary Element Method (BEM) to perform shape optimization. The advantage of exact boundary discretization favors IGABEM for shape optimization. IGABEM has been applied for acoustic shape optimization applications. Liu et al. (2017) applied shape optimization for sound barriers using the isogeometric fast multipole BEM. The required acoustic shape sensitivities with respect to control points were computed and the sound pressure minimization was selected as the design objective. Chen et al. (2018) performed shape and topology optimization to find the optimum distribution of acoustic absorbing material. Peake et al. (2013) applied extended isogeometric boundary element method (XIBEM) to solve two-dimensional Helmholtz problems. The use of XIBEM reduced the overall degrees of freedom approximately by 40% compared to the traditional BEM mainly due to the reduced system matrices. Simpson et al. (2014) performed acoustic IGABEM based on T-splines. The obtained solutions were compared with closed-form solutions and found to be superior. Some other applications of shape optimization using IGABEM can be found in Kostas et al. (2017), Sun et al. (2018), Henwood (1993), Dodgen and Khajah (2018). While BEM is very attractive for shape optimization of devices relying on wave propagation phenomena it suffers from the increased computational cost due to the dense linear system which limits its applications for high-frequency analysis as well as 3D analysis. Another challenge specific to BEM is the necessity to develop the analytical solution and deal with possible singularities. This makes IGA/FEM an easier adaptation for such applications especially with the recent developments in generating the required meshes. A detailed review of IGABEM, its applications, and limitations is presented in Ummidivarapu and Voruganti (2019).

This paper focuses on the study and application of shape optimization to an acoustic horn to transmit an incoming wave as efficiently as possible. Hence, the back reflection which is sensitive to the horn boundary shape should be minimized. Minimization of the reflections from an acoustic horn by shape optimization was studied previously. Bängtsson et al. (2003) performed the shape optimization of the acoustic horn using FEA and the gradient-based Broyden–Fletcher–Goldfarb–Shanno (BFGS) algorithm. The BFGS method belongs to quasi-Newton methods for which the necessary condition for optimality is the gradient to be zero. Both single and multi-frequency optimization were performed. A failed case of the three-frequency optimization due to the convergence issue was also reported. Barbieri and Barbieri (2013) performed the shape optimization of the acoustic horn using FEA and genetic algorithm (GA). The reflection coefficient was taken as the objective function. Single and two-frequency optimization were performed and the results obtained were compared with those of Bängtsson et al. (2003). Barbieri et al. (2015) performed the optimization of acoustic filters using particle swarm optimization (PSO). Problems analyzed involve parametric optimization of mufflers and shape optimization of acoustic horns. Morgans et al. (2008) employed a surrogate optimization method namely 'Efficient Global Optimization' for performing shape optimization of horn-loaded loudspeakers. Spline-based parameterization was used to represent the horn geometry. The obtained optimal shapes of the loudspeaker resulted in an improvement in sound quality for the listener. Similarly, other related studies on acoustic horn shape optimization can be found in Wadbro et al. (2010) and Schmidt et al. (2016). All the above studies employed FEA-based shape optimization to design an efficient horn by minimizing the reflection from the horn.

In the present work, in order to design an efficient acoustic horn, the objective function of the problem considered is precisely the same as in Barbieri and Barbieri (2013) (which used FEA and GA), but instead of FEA, we employ IGA

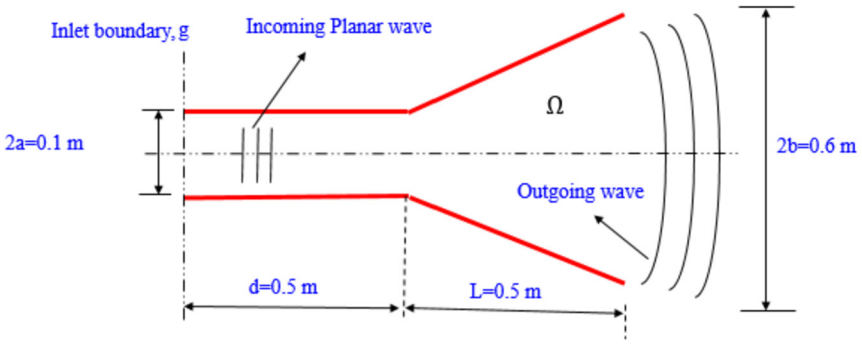

Fig. 1. The wave flow (left to right) along with geometric definitions of the unbounded 2-D acoustic horn model. The input plane wave enters the horn from the inlet boundary (g) of width $2a$, flows through the planar waveguide of length d, the conical horn section of length L, and leaves into the surrounding air as a cylindrical wave. The conical termination of the horn has a width of $2b$. The unbounded region (Ω) is the domain of analysis.

to perform analysis during shape optimization. For the optimization process, TLBO was employed. The main advantage of IGA in the context of shape optimization is the exact representation of the geometry and smooth representation of the boundaries. Furthermore, high order analysis ensures higher analysis accuracy. The above-mentioned studies successfully utilized shape optimization in IGA for various applications. A recent review article on isogeometric shape optimization can be found in Wang et al. (2018b).

TLBO is a recently proposed evolutionary-based optimization algorithm (Rao et al., 2011). The main advantage of TLBO over GA is the absence of algorithm-specific tuning parameters. In GA, the optimal selection of the rate of crossover and mutation for a specific problem is not a straightforward task. Unlike GA and many other evolutionary algorithms, there are no algorithm-specific parameters in TLBO which makes it simple and easy to use. TLBO has been applied to various applications. Toğan (2012) applied TLBO for designing planar steel frames. Here the objective was to obtain minimum weight frames subjected to strength and displacement requirements. Improved optimum solutions were found using TLBO when compared with other evolutionary algorithms. Camp and Farshchin (2014) applied TLBO for designing space trusses with discrete and continuous design variables. The objective function was the total weight of the structure subjected to strength and displacement limitations. The computational performance of TLBO was compared with other classical and evolutionary optimization methods and found to be better. Rao and Patel (2013) applied TLBO to multi-objective optimization of the two-stage thermoelectric cooler. The basic TLBO algorithm was modified slightly to improve the convergence rate. Rao et al. (2012) applied TLBO for large scale non-linear optimization problems. The TLBO algorithm performed better, with less computational effort for large scale problems, when compared with other popular optimization algorithms. Various applications of TLBO can be found in Rao (2016).

The acoustic horn considered in this study is shown in Fig. 1.

Isogeometric shape optimization of the acoustic horn using the TLBO algorithm involves three steps: (i) generation of the required computation model. The computational domain was presented using a multi-patch NURBS (Non-Uniform Rational B-Splines). The multi-patch technique was employed to generate the model. (ii) Perform acoustic analysis using IGA. IGA was used to compute the pressure distribution and the reflection coefficient R, which was taken as the objective function. (iii) Find the optimum solution using the TLBO algorithm. The objective function, i.e. the reflection coefficient, R, was evaluated in the IGA platform as a function of the location of the control points controlled by the TLBO algorithm and minimized over iterations. Minimizing R has a significant effect on the overall reflection spectra of the horn.

2. The problem statement

We consider the acoustic horn shown in Fig. 1 for the shape optimization process. For simplicity, it is assumed that this horn speaker extends infinitely in the direction normal to the plane. Within the waveguide we consider a monochromatic planar wave propagating from left to right. It is assumed that all other non-planar modes are evanescent in the waveguide. When the planar wave reaches the conical portion, some of its energy is reflected back yielding a reflected wave. When these reflected and incoming waves interfere, superposition occurs leading to the formation of bands which decreases the efficiency of horn loudspeakers. This can be avoided or reduced by shape optimization of the horn profile.

The present study focuses on the horn with mirror symmetry about the plane passing through the centreline of the waveguide. The domain of analysis is the surrounding medium (Ω) as shown in Fig. 1. Any domain (Ω) to be analyzed should be bounded. In the present study, the computational domain was artificially truncated at a radius $R_\Omega = 1$ m identical to the study conducted by Bängtsson et al. (2003) and examples provided in Barbieri and Barbieri (2013). The corresponding symmetric bounded model of the acoustic horn is shown in Fig. 2. All the other dimensions of the horn model are given in Fig. 1. The domain of analysis (Ω) is shown in Fig. 2 as well as all the boundaries ($\mathbb{\Gamma}$) of the model, and the radius of truncation (R_Ω). Among all the boundaries, the boundary $\mathbb{\Gamma}_d$, shown with the dotted red line is the design boundary which changes during optimization. Finally, the problem of shape optimization is defined as finding the optimal design boundary, $\mathbb{\Gamma}_d$, for which the reflection is minimum.

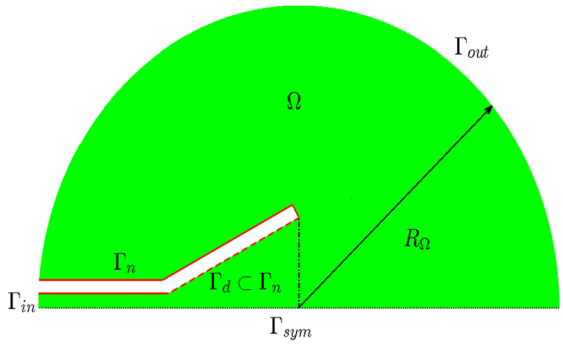

Fig. 2. Bounded computational acoustic horn model showing the definitions of the design and the domain regions. Γ_{in} is the inflow boundary through which the wave enters the waveguide. Γ_{out} is an artificial boundary created to truncate the outer unbounded space. Γ_{n} is the boundary of the structural horn. Γ_{d} is a subset of Γ_{n} and is the design boundary that changes during the optimization process. Γ_{sym} is the boundary of symmetry. Ω is the domain of analysis. R_Ω is the radius of the truncation of the bounded domain. (For interpretation of the colors in the figure(s), the reader is referred to the web version of this article.)

Consider the initial incoming wave of frequency f and amplitude A. Let $M(\boldsymbol{x}, t)$ be the pressure distribution generated by this incoming wave where $\boldsymbol{x}$ is the spatial coordinate (x, y) and t is the instant of time. Let $N(\boldsymbol{x}, t)$ be the pressure distribution of the reflected wave which is a function of the design boundary, Γ_{d}, of the horn. Assuming only planar waves are present in the waveguide, the resultant pressure, P, of the two waves can be expressed as

$$P(\boldsymbol{x}, t) = M(\boldsymbol{x}, t) + N(\boldsymbol{x}, t) \tag{1}$$

Assuming that the acoustical pressure, $P(\boldsymbol{x}, t)$, is governed by the wave equation

$$\frac{\partial^2 P}{\partial t^2} = c^2 \Delta P \tag{2}$$

where c is the speed of sound and Δ denotes the Laplacian operator. The general solution to the equation (2) can be expressed as

$$P(\boldsymbol{x}, t) = Ae^{i(k\boldsymbol{x}\boldsymbol{n}+\omega\boldsymbol{t})} + Be^{i(-k\boldsymbol{x}\boldsymbol{n}+\omega\boldsymbol{t})} \tag{3}$$

where ω is the angular frequency, $k = \omega/c$ is the wavenumber, A and B are the amplitudes of input and reflected waves and $\boldsymbol{n}$ denotes the outward-directed unit normal on the boundary of Ω. Making use of the ansatz, $P(\boldsymbol{x}, t) = p(\boldsymbol{x})e^{i\omega t}$ and taking into consideration appropriate boundary conditions-see (Bängtsson et al., 2003; Barbieri and Barbieri, 2013), for detailed discussion, the *Helmholtz equation* for the complex amplitude function, $p(\boldsymbol{x})$, can be expressed as,

$$c^2 \Delta p + \omega^2 p = 0 \quad \text{in } \Omega \tag{4}$$

$$\left(i\omega + \frac{c}{2R_\Omega}\right) p + c\frac{\partial p}{\partial n} = 0 \quad \text{on } \Gamma_{out} \tag{5}$$

$$i\omega p + c\frac{\partial p}{\partial n} = 2i\omega A \quad \text{on } \Gamma_{in} \tag{6}$$

$$\frac{\partial p}{\partial n} = 0 \quad \text{on } \Gamma_n \cup \Gamma_{sym} \tag{7}$$

2.1. Modeling of the computational domain

The above equation system is to be solved for the amplitude function, p, over the acoustic model shown in Fig. 2. The first step is to develop the required computational model. NURBS (Non-Uniform Rational B-splines) was used to develop the computational model shown in Fig. 2.

NURBS is a generalization of B-splines. B-splines are generated with the help of control points and the basis functions. The entire geometry is constructed in a parametric space ranging from (0–1). The parametric region is divided into intervals (knot spans) using knot vectors. A knot vector $\boldsymbol{\xi} = \{\xi_1, \xi_2, \ldots, \xi_{n+p+1}\}$ is a non-decreasing sequence of parameter values, where n is the number of basis functions and p is the degree of the basis. The basis functions are built using the following recursive relations. Given a knot vector $\boldsymbol{\xi}$, the $\boldsymbol{i}$th ($\boldsymbol{i} = 1$ to n) basis function of zeroth degree ($p = 0$) is given by Piegl and Tiller (2012),

$$N_{\boldsymbol{i},0}(\xi) = \begin{cases} 1, & \xi_{\boldsymbol{i}} \le \xi < \xi_{\boldsymbol{i}+1} \\ 0, & \text{otherwise} \end{cases} \tag{8}$$

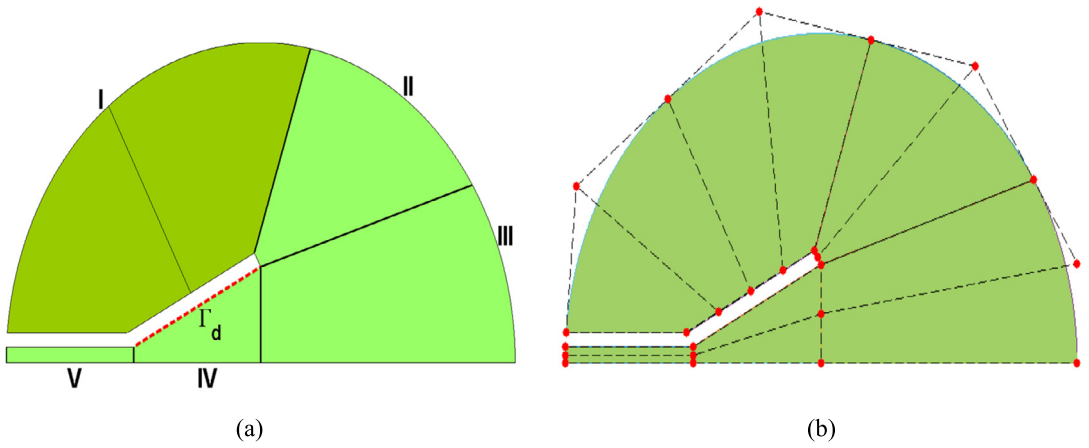

Fig. 3. The initial coarse mesh of the acoustic horn developed using NURBS. (a) Five patches (I, II, III, IV, and V). The design boundary, $\mathbb{\Gamma}_{\mathrm{d}}$, shown with the dotted red line is present in patch 4. Note that the I$^{\mathrm{st}}$ patch has two elements. (b) Corresponding control points of the mesh shown with red dots.

and for $p > 0$

$$N_{\boldsymbol{i},p}(\xi) = \frac{\xi - \xi_{\boldsymbol{i}}}{\xi_{\boldsymbol{i}+p} - \xi_{\boldsymbol{i}}} N_{\boldsymbol{i},p-1}(\xi) + \frac{\xi_{\boldsymbol{i}+p+1} - \xi}{\xi_{\boldsymbol{i}+p+1} - \xi_{\boldsymbol{i}+1}} N_{\boldsymbol{i}+1,p-1}(\xi) \tag{9}$$

Considering the B-spline basis functions, $N_{\boldsymbol{i},p}(\xi)$ and their corresponding weights, $w_{\boldsymbol{i}}$, NURBS basis functions, $R_{\boldsymbol{i},p}(\xi)$, are defined as

$$R_{\boldsymbol{i},p}(\xi) = \frac{N_{\boldsymbol{i},p}(\xi)\, w_{\boldsymbol{i}}}{\sum_{\boldsymbol{i}=1}^{n} N_{\boldsymbol{i},p}(\xi)\, w_{\boldsymbol{i}}} \tag{10}$$

where $R_{\boldsymbol{i},p}(\xi)$ are the rational basis functions. Using these basis functions, a NURBS curve can be defined as,

$$\mathbb{C}(\xi) = \sum_{\boldsymbol{i}=1}^{n} R_{\boldsymbol{i},p}(\xi)\, B_{\boldsymbol{i}} \tag{11}$$

where, n is the number of control points, $B_{\boldsymbol{i}}$.

Similarly, NURBS surfaces $\mathbb{S}(\xi,\eta)$ can be defined in a two-parameter space (ξ and η) (Piegl and Tiller, 2012). Let p and q be the degree of the basis in each parametric direction respectively. We denote the number of control points in the corresponding parametric directions by n and m respectively. Using the bidirectional net of control points $\{B_{\boldsymbol{ij}}\}$ with their corresponding weights w_{ij} and the product of the univariate B-spline basis functions, the NURBS surface $\mathbb{S}(\xi,\eta)$ can be obtained as

$$\mathbb{S}(\xi,\eta) = \frac{\sum_{i=1}^{n}\sum_{j=1}^{m} N_{\boldsymbol{i},p}(\xi)\, N_{\boldsymbol{i},q}(\eta)\, w_{ij} B_{\boldsymbol{ij}}}{\sum_{i=1}^{n}\sum_{j=1}^{m} N_{\boldsymbol{i},p}(\xi)\, N_{\boldsymbol{i},q}(\eta)\, w_{ij}} \tag{12}$$

If the piecewise rational basis functions $R_{\boldsymbol{i},j}(\xi,\eta)$ are introduced as

$$\mathrm{R}_{\boldsymbol{i},\boldsymbol{j}}(\xi,\eta) = \frac{N_{\boldsymbol{i},p}(\xi)\, N_{\boldsymbol{i},q}(\eta)\, w_{ij}}{\sum_{k=1}^{n}\sum_{l=1}^{m} N_{\boldsymbol{k},p}(\xi)\, N_{\boldsymbol{l},q}(\eta)\, w_{kl}} \tag{13}$$

Then, the NURBS surface in equation (12) can be written as,

$$\mathbb{S}(\xi,\eta) = \sum_{i=1}^{n}\sum_{j=1}^{m} \mathrm{R}_{\boldsymbol{i},\boldsymbol{j}}(\xi,\eta)\, B_{\boldsymbol{ij}} \tag{14}$$

Using the above relations of NURBS basis functions, the horn computational model was developed. A 5-patch mesh of the horn model is shown in Fig. 3(a). By representing the domain with multi-patches, the design boundary ($\mathbb{\Gamma}_{\mathrm{d}}$) was described by the patch 4 only.

Initially, each patch is defined with the orders of 2×1 i.e., quadratic in one direction and linear in other. Each patch consists of single elements except patch 1 which has two elements. Fig. 3(b) shows the corresponding control points of the mesh. The patch wise list of control points along with the knot vectors of the coarse mesh is provided in Appendix A.

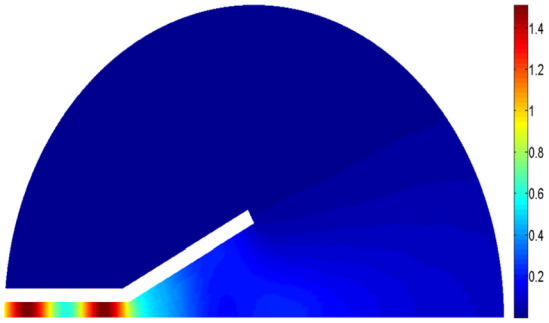

Fig. 4. The square of the absolute value of the sound pressure ($|p_h|^2$) inside the computational domain. The formation of the bands in the waveguide demonstrates undesirable reflection.

2.2. Acoustic analysis of the computational domain

The system of acoustic equations (4)–(7), is to be solved over the developed computational model. In order to obtain the variational formulation for this system of equations, the solution, p, is approximated in space $V_h = span\{R_j\} \subset H^1(\Omega_h)$ where R_j are the NURBS basis functions, $H^1(\Omega_h)$ is a space of square-integrable complex-valued functions. Multiplying V_h with the elliptic equation (4) and integrating by parts gives the required weak form Barbieri and Barbieri (2013) as below,

$$c^2 \int_{\Omega_h} \nabla R_j . \nabla p_h d\Omega - \omega^2 \int_{\Omega_h} R_j p_h d\Omega + i\omega c \int_{\Gamma_{in} \cup \Gamma_{out}} R_j p_h d\Gamma + \frac{c^2}{2R_\Omega} \int_{\Gamma_{out}} R_j p_h d\Gamma = 2i\omega c A \int_{\Gamma_{in}} R_j d\Gamma \tag{15}$$

The above equation (15) was discretized using NURBS basis functions and solved for the amplitude function, p_h, using GeoPDEs 3.0 (Vázquez, 2016). It was shown that accurate results can be obtained in high order IGA with minimal pollution error even in mid to high-frequency range (Khajah et al., 2017, 2018; Khajah and Villamizar, 2019; Videla et al., 2019; Xu et al., 2019). In order to increase the accuracy of the analyses, k-refinement was performed for the entire domain. First, the bases were degree-elevated to biquintics and then the knot-insertion was performed by dividing each knot span into 5 subdivisions. The total number of elements present in the refined analysis mesh was 150. The patch wise element list is as follows: Patch 1: 50, Patch 2: 25, Patch 3: 25, Patch 4: 25 and Patch 5: 25.

The computed square of the absolute value of the sound pressure, $|p_h|^2$, is shown in Fig. 4 for frequency $f = 550$ Hz, and Amplitude $A = 1$ m. The speed of sound was assumed to be $c = 340$ m/s. The generation of the bands can be seen in the waveguide which indicates reflection. These bands are generated due to the superposition of the incoming and reflected waves. For the loudspeakers, these bands create disturbances in the overall sound quality and hence should be avoided.

2.3. Objective function

From Fig. 4, it is clear that the task of shape optimization is to modify the shape of Γ_d (see Fig. 3(a) for boundary definition), such that the reflected wave component is minimized. The objective function for the shape optimization follows (Barbieri and Barbieri, 2013). The reflection coefficient, R, which is defined as the quotient between the amplitude of the reflected wave (B) and the incoming wave (A) was taken as the objective function.

$$R = B/A \tag{16}$$

In the present work, the amplitude of input wave (A) was taken as 1 m. The total amplitude (p) at the inflow boundary can be written as, $p = A + B$. Therefore, the magnitude of the reflected wave on the inflow boundary, Γ_{in}, can be written as $B = p - A$. Denoting by $p(\mathbf{0}) = p(0,0)$ the value of $p(\boldsymbol{x})$ in Γ_{in}, the objective function, f, can be defined as

$$min\ f = |p(\mathbf{0}) - A| \tag{17}$$

If $f = 0$, then $p = A$, and therefore, the reflection, $B = 0$. Since $A = 1$, $R = f$. The reflection coefficient, R is independent of the input amplitude A. It is the measure of the fraction of the incoming wave that reflected back. Equation (17) is the objective function for single-frequency optimization. The objective function formulation of multi-frequency optimization is presented in section 3. Several optimization algorithms were used for acoustic horn shape optimization in previous studies (Bängtsson et al., 2003; Barbieri and Barbieri, 2013; Barbieri et al., 2015; Morgans et al., 2008; Wadbro et al., 2010; Schmidt et al., 2016). In the present work, TLBO was used to control the design variables in order to obtain minimum reflection.

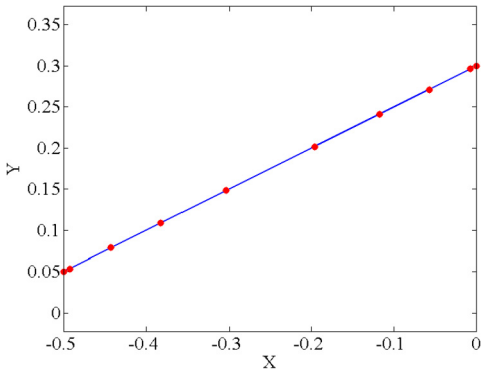

Fig. 5. The reference design boundary, $\mathbb{\Gamma}_{dR}$, modeled with 10 control points shown with red dots. The boundary's interior 8 control points are used as design variables.

Table 1
The coordinates of the control points defining the reference design boundary, $\mathbb{\Gamma}_{dR}$.

Control point	X-Coordinate	Y-Coordinate
1	−0.5	0.05
2	−0.48	0.06
3	−0.44	0.08
4	−0.38	0.11
5	−0.3	0.15
6	−0.2	0.2
7	−0.12	0.24
8	−0.06	0.27
9	−0.02	0.29
10	0	0.3

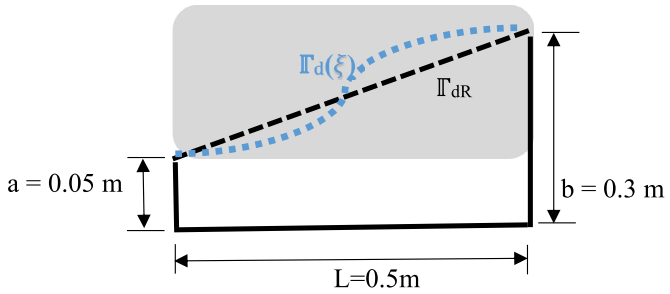

Fig. 6. The design space in the grey background showing the possibilities of the design boundaries $\mathbb{\Gamma}_d(\xi)$. $\mathbb{\Gamma}_{dR}$ represents the reference design boundary.

2.4. The optimization model and the design space

For the optimization purpose, patch 4 which contains the design boundary ($\mathbb{\Gamma}_d$) was reconstructed. In the process, the reference design boundary, $\mathbb{\Gamma}_{dR}$, was defined using 10 control points as shown in Fig. 5. The coordinates of the control points are shown in Table 1. The degree of the basis functions in the parametric direction ($\boldsymbol{\xi}$) in which the design boundary ($\mathbb{\Gamma}_{dR}$) was defined was set to 5. The interior 8 control points were used as design variables during optimization.

The effective geometric modeling of the design boundary $\mathbb{\Gamma}_d$ leads to efficient results as already stated that the horn reflections are very sensitive to the horn boundary. There are numerous possibilities of $\mathbb{\Gamma}_d$ in the design space provided. In the present study, a particular design boundary ($\mathbb{\Gamma}_d$) is defined using a set of control points and their corresponding NURBS basis functions as

$$\mathbb{\Gamma}_d = \sum_{i=1}^{n} B_{\boldsymbol{i}} R_j \tag{18}$$

where, $B_{\boldsymbol{i}}$ are the control points, n is the number of control points and R_j are the corresponding basis functions. A given set of control points, B_i, defines a particular design boundary. Hence, the control points, B_i, are the design variables which change during optimization. The bounds on the design variables define the scope of the design space. The design space is shown in the grey background in Fig. 6.

3. TLBO algorithm

TLBO algorithm is a recently proposed evolutionary algorithm, which mimics the classroom environment for the optimization process. It is a simple, robust and fast converging algorithm. The main advantage of the TLBO algorithm is the absence of algorithm-specific tuning parameters like crossover and mutation rate in GA and acceleration constants in PSO. TLBO is a simple algorithm and it consists of two phases namely teacher and learner phase.

In the TLBO algorithm, the number of students of a classroom (C) is treated as population size (P). The subjects are analogous to the design variables (X). The total marks scored in all the subjects by each student is the fitness value of that particular population in that generation. A particular design variable of an ith member of the population is referred to as X_{ij}. After initializing the random values of design variables for all the population, the fitness values are computed for each population according to the objective function. The student with the best fitness value among the population is identified as the teacher. The corresponding design variables of the teacher, $X_{teacher\,j}$, are noted. Using this, the overall performance of the entire population is increased in two ways: (1) The teacher, tries to improve the performance of the students called as 'Teacher phase' and (2) Students discuss among themselves to improve their overall performance called as 'Learner phase'.

3.1. Teacher phase

In this phase, the teacher increases the performance of the overall population. Let r be the random number between 0 and 1. First, the mean values, M_j, of each subject for all students are computed i.e., the mean of each design variable for all the population is found. Then the old values of the design variables, X_{ijold}, of the individual population are replaced with the new values, X_{ijnew}, using the following relation (Rao et al., 2011):

$$X_{ijnew} = X_{ijold} + r(X_{teacher\,j} - M_j) \tag{19}$$

This is repeated for the entire population. After updating the design variables, the fitness values of the population are computed and are compared with the old fitness values. Among them, the best fitness values and their corresponding design variables are collected. This ends the teacher phase.

3.2. Learner phase

In this phase, the students improve themselves by interacting among themselves. After the teacher phase, randomly, two populations (m, n) are selected and their fitness values (f_m and f_n) are compared. The design variables are modified according to

$$\begin{aligned} X_{ijnew} &= X_{ijold} + r\left(X_{mj} - X_{nj}\right) \quad \text{if } f_m < f_n \\ X_{ijnew} &= X_{ijold} + r\left(X_{nj} - X_{mj}\right) \quad \text{if } f_n < f_m \end{aligned} \tag{20}$$

This is repeated for the entire population. These modified values of the design variables are used to compute the new fitness values. The fitness values of the set obtained in the learner phase are compared with that of the teacher phase and the best solutions are selected among them. In the end, the best fitness value among the population is selected as the best solution for the current iteration. This ends the learner phase. This procedure is repeated until the convergence criterion is reached.

3.3. Acoustic horn shape optimization using TLBO algorithm

For all single and multi-frequency optimization, the y-coordinates of 8 control points of the design boundary ($\mathbb{\Gamma}_{\mathrm{d}}$) shown in Fig. 7 were taken as design variables. By taking only y-coordinates as design variables, the possibility of mesh distortion was reduced when combined with the corresponding movement of internal control points. Therefore, 8 design variables were considered in this study. The design boundary has higher continuity (C^{p-1}) due to the high order basis functions except at the endpoints which were not considered as design variables. The upper and lower bound of the design variables were uniformly selected to be ± 0.04 resulting in the variation limits presented in Table 2.

In the single-frequency optimization, as stated earlier in Equation (17), the objective function is the reflection coefficient, R. The R has to be minimized by changing the shape of the horn through updating the location of the design variables controlled by TLBO algorithm. In multi-frequency optimization, two or more frequencies were considered simultaneously. Here, the optimization aims to find a unique horn shape that is optimal for all the frequencies considered. This is not a straightforward task since a shape optimal for one frequency might not be optimal for the others. Hence, it forms a multi-objective optimization problem. In this study, two-frequency and three-frequency optimization were considered.

The formulation of the multi-objective optimization problem is as follows: consider two frequencies denoted by F_1 and F_2. Suppose Op_1 and Op_2 are the respective optimal values obtained for F_1 and F_2 in single-frequency optimization. The normalized objective functions for multi-objective optimization are defined as

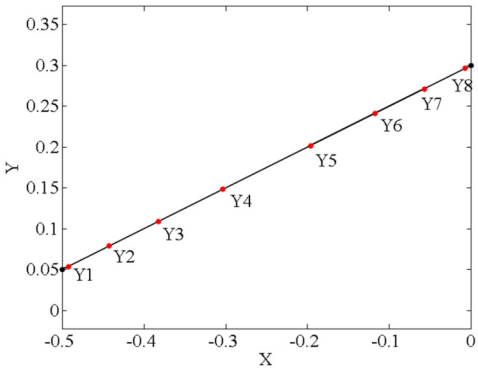

Fig. 7. The reference design boundary, $\mathbb{\Gamma}_{dR}$, showing the design variables (Y1–Y8). The design variables are the y-coordinates of the 8 control points shown in red color. The extreme control points shown in black are fixed during optimization.

Table 2
Upper and lower bounds of the design variables.

Design variable	Upper bound	Lower bound
Y1	0.1	0.02
Y2	0.12	0.04
Y3	0.15	0.07
Y4	0.19	0.11
Y5	0.24	0.16
Y6	0.28	0.2
Y7	0.31	0.23
Y8	0.33	0.25

$$Normalobj_1 = \frac{Obj_1}{Op_1}$$
$$Normalobj_2 = \frac{Obj_2}{Op_2} \tag{21}$$

The normalization is carried out to ensure that both of the objectives are of a uniform scale. Then the final multi-objective function is formulated as

$$Multiobj = w_1 \times Normalobj_1 + w_2 \times Normalobj_2 \tag{22}$$

where w_1 and w_2 are the weights. In our study, equal weights were considered i.e. $w_1 = w_2 = 0.5$. A similar formulation can be carried out for any multi-frequency optimization.

4. Shape optimization results

4.1. Single-frequency optimization

The horn was optimized for 4 single frequencies independently. The optimum horn shape was found for 280, 400, 550, and 780 Hz frequencies. Based on a few trials and errors on the objective function value, the population size and the maximum number of iterations considered for the study were 10 and 50 respectively. The optimization program was run for one or more times to obtain the smooth optimal shape. The smoothness of the shape obtained was inspected visually for manufacturability.

The optimum shape of the design boundary of the horn for frequency 550 Hz is shown in Fig. 8(a). The acoustic analysis was performed and the square of the absolute value of the sound pressure ($|p_h|^2$) is shown in Fig. 8(b). There are no visible bands in the waveguide in Fig. 8(b) which illustrates no or minimum reflection which shows a considerable improvement when compared to the initial design presented in Fig. 4.

The objective function values of the IGA-TLBO were compared with published results of FEM-GA (Barbieri and Barbieri, 2013) in Table 3 obtained for a domain truncated at 1 m radius. The optimum solution found using IGA-TLBO reduces the value of the objective function more than those of FEM-GA. The GA characteristics are number of bits=12; number of elements by generation=25; maximum number of iterations=50; elitist reproduction; cross probability=0.05; and mutation rate=0.02. In FEM-GA (Barbieri and Barbieri, 2013), the number of design variables for single-frequency optimization considered were 3.

The comparative results for the reflection coefficient, R, as a function of frequency are shown in Fig. 9 which is often referred to as the reflection spectrum. A reflection spectrum provides the variation of R for a particular horn shape over

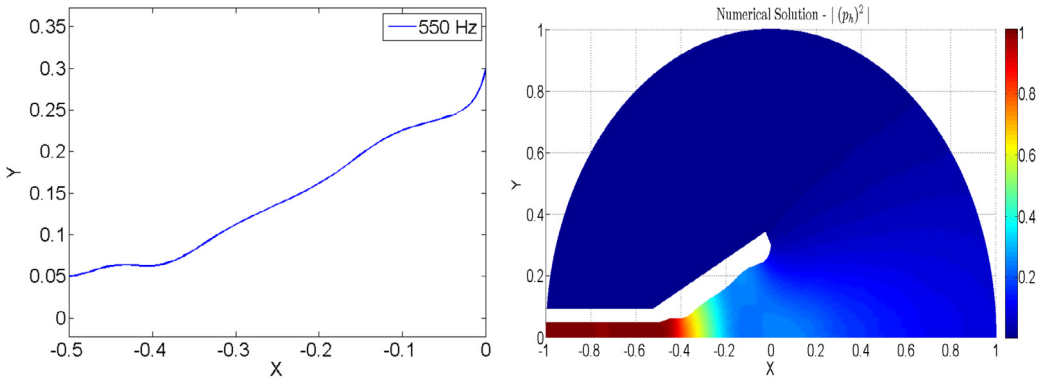

Fig. 8. Single-frequency optimization results. (a) Optimal design boundary for 550 Hz frequency. (b) The square of the absolute value of the sound pressure ($|p_h|^2$) in the acoustic horn with no visible bands in the waveguide indicating no or minimal reflection.

Table 3
Results of single-frequency optimization comparing IGA-TLBO with FEM-GA (Barbieri and Barbieri, 2013).

Frequency	Objective function (R) value using IGA-TLBO	Objective function (R) value using FEM-GA (Barbieri and Barbieri, 2013)
280	**9.7683e-08**	5.2903e-05
400	**8.9054e-08**	5.4937e-05
550	**9.6784e-08**	4.3822e-06
780	**1.4491e-07**	3.9092e-05

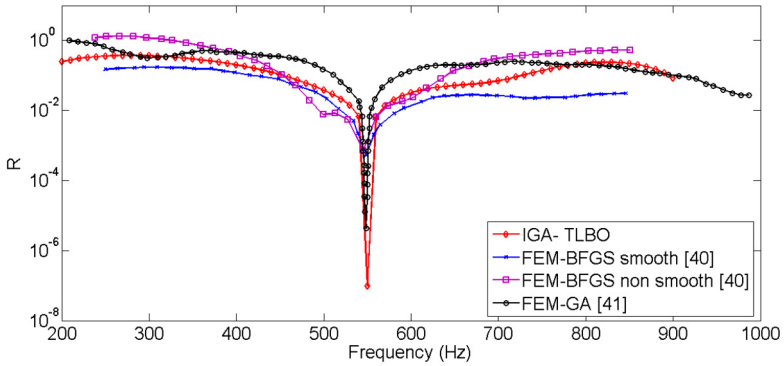

Fig. 9. Comparative results of reflection coefficient R, as a function of frequency (Hz). The reflection is further reduced using IGA-TLBO compared to FEM-based optimization.

the entire frequency range. The reflection spectra obtained by IGA-TLBO in this study were improved when compared to FEM-GA (Barbieri and Barbieri, 2013) and FEM-BFGS (Bängtsson et al., 2003) as illustrated in Fig. 9.

Fig. 10 shows the results on the axis of symmetry and it can be observed that for the initial shape, the amplitude of $|p(x,0)|$ varies along the waveguide (x ranging from -1 to -0.5), indicating the presence of the reflected wave, $B \neq 0$, so as the bands exist as shown in Fig. 4. For the obtained optimal shape, it can be noticed that $|p(x,0)| \approx 1$ along the waveguide resulting in minimal reflection i.e. $B = 0$. Hence, no bands are observed in the waveguide as shown in Fig. 8(b).

Similarly, the design boundaries of 280, 400 and 780 Hz are shown in Fig. 11(a). The respective reflection spectra were compared with that of FEM-BFGS (Bängtsson et al., 2003) in Fig. 11(b). From the figure, it can be observed that IGA-TLBO produced better reflection spectra compared to FEM-BFGS. The optimum values of the design variables for all the cases of single-frequency optimization are presented in Table 4.

4.1.1. Mesh dependency test

The results reported in the present study correspond to the design boundary ($\mathbb{\Gamma}_d$) defined using the non-uniform distribution of control points as seen from Fig. 7. From the literature, it was found that the optimal solution of a shape optimization problem depends on the number of the design variables (control points) as well as their distribution on the design boundary ($\mathbb{\Gamma}_d$). To study this, a design boundary with uniform distribution of 10 control points was generated and

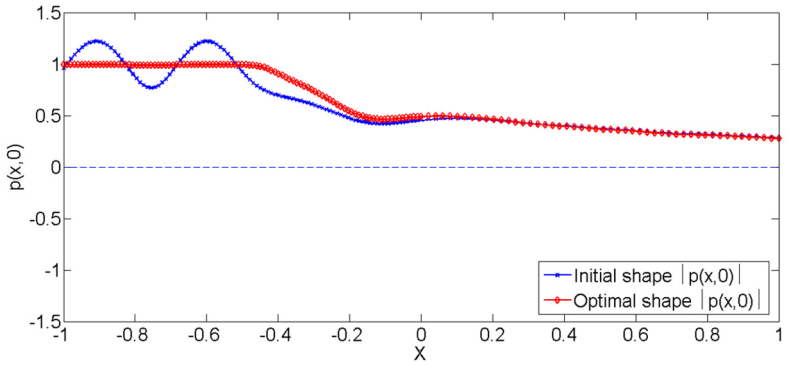

Fig. 10. Values of $p(x, 0)$ for the frequency of 550 Hz.

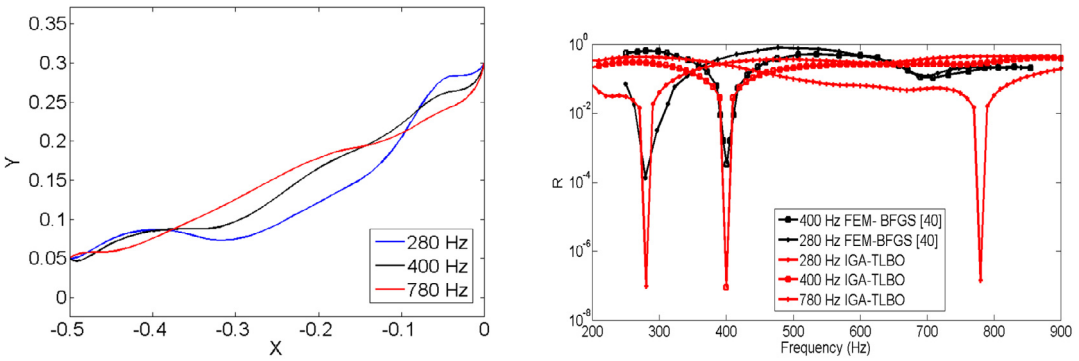

Fig. 11. (a) Optimal design boundaries of the single-frequency optimization (280, 400 and 780 Hz). (b) Corresponding reflection spectra compared with that of FEM-BFGS (Bängtsson et al., 2003). IGA-TLBO produced better reflection spectra compared to FEM-BFGS.

Table 4
Optimal design variables for single-frequency optimization.

Design variable	Initial position	Optimal position (280 Hz)	Optimal position (400 Hz)	Optimal position (550 Hz)	Optimal position (780 Hz)
Y1	0.06	0.0564	0.0504	0.0540	0.0571
Y2	0.08	0.0788	0.0738	0.0634	0.0605
Y3	0.11	0.0856	0.0872	0.0667	0.0848
Y4	0.15	0.0744	0.0969	0.1122	0.1258
Y5	0.2	0.1215	0.1650	0.1619	0.1786
Y6	0.24	0.1772	0.2073	0.2162	0.2009
Y7	0.27	0.2692	0.2553	0.2375	0.2336
Y8	0.29	0.2848	0.2687	0.2558	0.2569

the shape optimization was performed for the frequency of 550 Hz by selecting the interior 8 control points as design variables. Fig. 12(a) shows the uniform distribution of the control points. The optimal objective function value obtained was **1.7180e-06** which was different from the one obtained using the non-uniform distribution of control points which was **9.6784e-08**. The optimal shape obtained for both cases was also different. The acoustic analysis of the obtained optimal shape for the uniform distribution case is shown in Fig. 12(b).

Hence, the optimal solution changes if the distribution of the control points is changed. In the present study, the non-uniform distribution case gave better results when compared to the uniform distribution case. The optimal solution was also analyzed for a different number of design variables. For this, a mesh dependency test was performed for three sets of design variables (6, 8 and 10) which are uniformly distributed on the design boundary ($\mathbb{\Gamma}_d$) of the horn. The corresponding reflection spectra and the optimal shapes for the 3 cases (6, 8 and 10 design variables (DV)) considered are depicted and compared in Fig. 13(a), and Fig. 13(b) respectively.

In all three cases, the objective function values are found to be in the order of 10^{-6} as observed from Fig. 13(a). Different optimal shapes were found in each case. It was found that the acoustic horn is very sensitive to even a minor change in the boundary. Furthermore, the results of this study confirm previous observations reported in the literature that there are

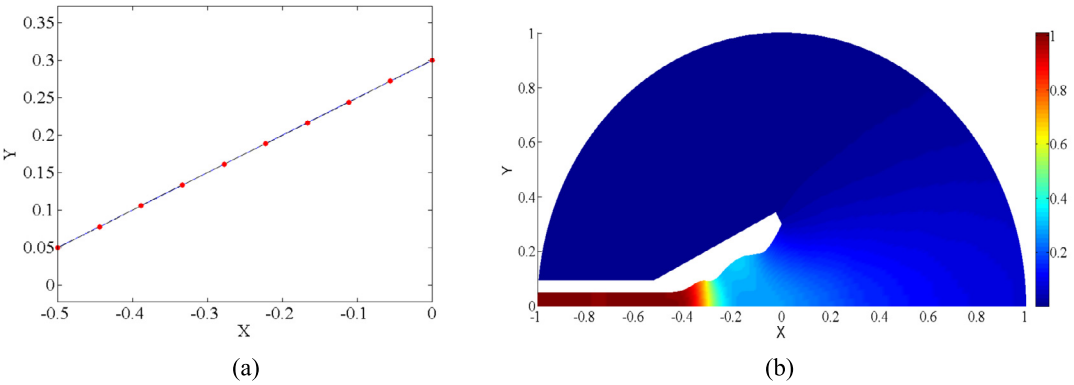

Fig. 12. (a) The design boundary discretized with uniform distribution of control points. (b) The acoustic analysis of the obtained optimal horn. The square of the absolute value of the sound pressure ($|p_h|^2$) in the acoustic horn with no visible bands in the waveguide indicating minimal reflection.

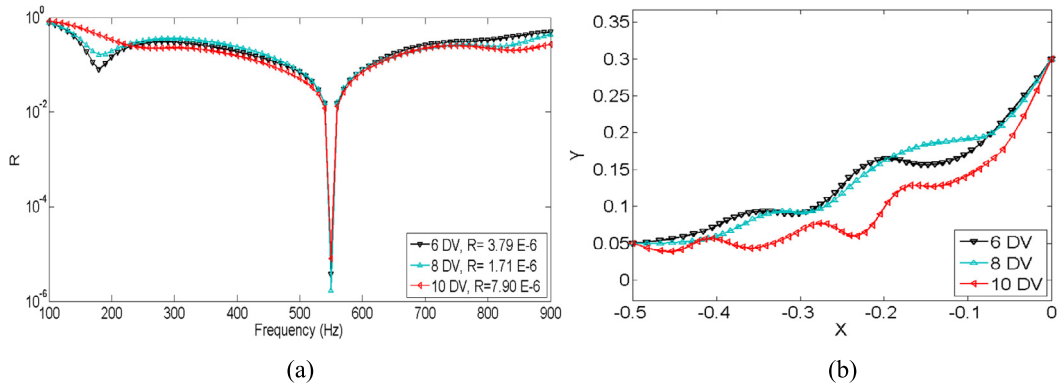

Fig. 13. (a) The computed reflection spectra of the optimal shapes obtained for the input frequency of 550 Hz using the three different set of design variables. (b) The optimal shapes corresponding to the three sets of design variables.

possibilities of getting more than one optimal shape for a given frequency (Bängtsson et al., 2003). For the case with 10 design variables, the optimal shape is wigglier. Hence, it is not desirable to model the design boundary with a high number of design variables than necessary. In case, if wiggly shapes are found by using a high number of design variables, a smooth design can be achieved by using a smoothing algorithm such as Tikhonov regularization (Mair, 1994).

Apart from the above studies, initially, shape optimization was performed by considering both the x and y-coordinates of the control points as design variables and compared the results with those found using y-coordinates only. It was observed for a fixed population size and number of iterations, lower objective function values were found when y-coordinates alone were considered as the optimization design variables. The movement of x-coordinates in the design space led to increased mesh distortion. Also, the inclusion of x-coordinates as optimization variables decreased the convergence speed due to the increased number of design variables. Hence, only y-coordinates of the control points were considered as design variables in the present study.

4.2. Two-frequency optimization

4.2.1. 350–450 Hz frequency

Shape optimization was performed for two frequencies (350 and 450 Hz) simultaneously. The analysis and optimization parameters were similar to single-frequency optimization. As discussed earlier, the challenge in multi-frequency optimization is that a particular shape optimal for one frequency might not be optimal for another. Therefore, arriving at a shape that is optimal for both the frequencies considered indicates the efficiency of the optimization algorithm. The employed TLBO algorithm produced improved results for multi-frequency optimization.

The optimal design boundary for the two-frequency (350 and 450 Hz) optimization is shown in Fig. 14(a). The numerical values of the objective function, f, are 1.0827e-07 and 1.2751e-09 for 350 and 450 Hz respectively. The corresponding reflection spectrum obtained by IGA-TLBO was compared with the literature and found to be better than the FEM-GA (Barbieri and Barbieri, 2013) and FEM-BFGS (Bängtsson et al., 2003) as shown in Fig. 14(b). The number of design variables used in IGA-TLBO, FEM-GA (Barbieri and Barbieri, 2013) and FEM-BFGS (Bängtsson et al., 2003) were 8, 8 and 29 respectively.

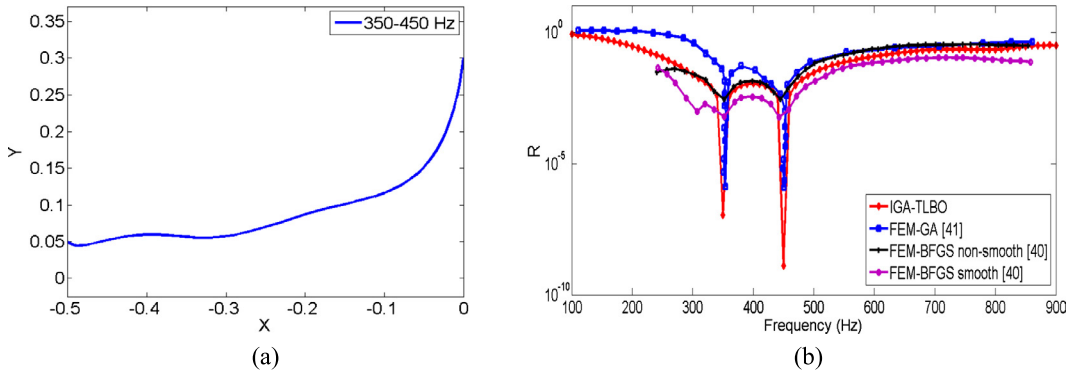

Fig. 14. (a) Optimal design boundary for the two-frequency (350–450 Hz) optimization using IGA-TLBO. (b) The comparison of the reflection spectra of IGA-TLBO with FEM-GA and FEM-BFGS.

Table 5
Optimal design variables for two-frequency optimization.

Design variable	Initial position	Optimal position (350–450 Hz)	Optimal position (600–800 Hz)
Y1	0.06	0.0451	0.0583
Y2	0.08	0.0544	0.0630
Y3	0.11	0.0592	0.0828
Y4	0.15	0.0574	0.1225
Y5	0.2	0.0868	0.1608
Y6	0.24	0.1092	0.1832
Y7	0.27	0.1414	0.1943
Y8	0.29	0.2060	0.2600

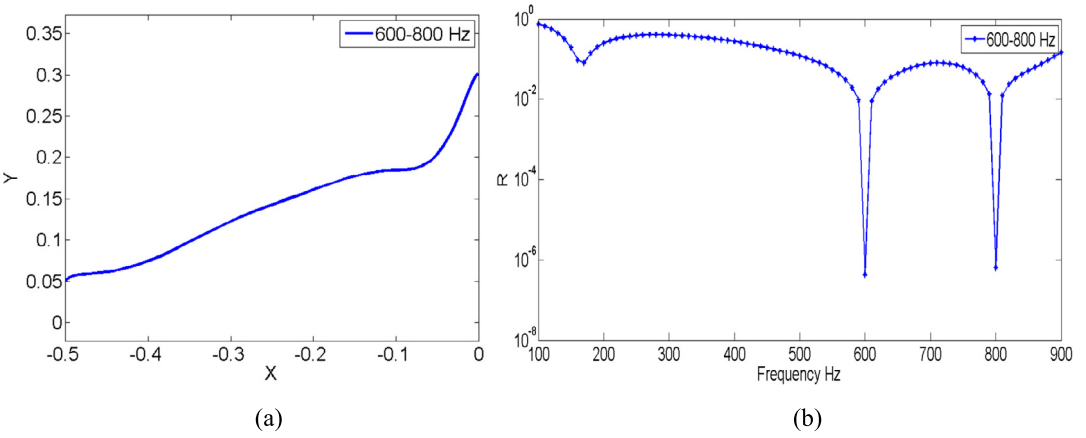

Fig. 15. (a) Optimal design boundary for the two-frequency (600–800 Hz) optimization. (b) The corresponding reflection spectrum.

4.2.2. 600–800 Hz frequency

Similarly, an additional case of 600 and 800 Hz frequency was also performed and the obtained results are presented. The optimal design boundary is shown in Fig. 15(a) with the corresponding reflection spectrum in Fig. 15(b). The numerical values of the objective function, f, are 4.2456e-07 and 6.3705e-07 for 600 and 800 Hz respectively. No results were available in the literature for comparison. The values of the design variables defining the optimal horn boundary obtained for two-frequency optimization are presented in Table 5.

4.3. Three-frequency optimization (400–600–800 Hz)

In the literature, no successful results were reported for three-frequency (400–600–800 Hz) optimization. Bängtsson et al. (2003) reported failed results which were caused due to the mesh corruption when solving the three-frequency optimization problem. In order to obtain the optimal solution, Bängtsson et al. (2003) refined the computational model to a much finer

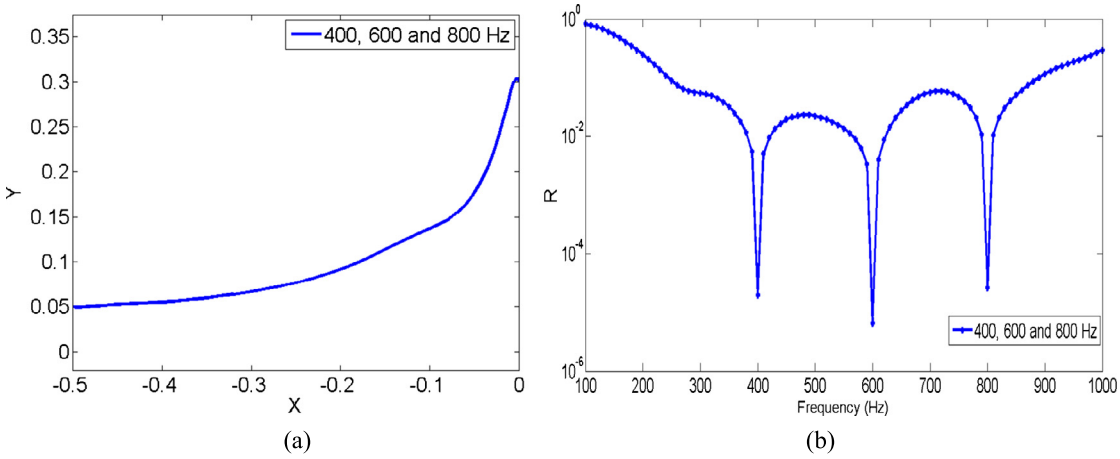

Fig. 16. (a) Optimal design boundary for the three-frequency (400, 600 and 800 Hz) optimization. (b) The corresponding reflection spectrum.

Table 6
Optimal design variables for three-frequency optimization.

Design variable	Initial position	Optimal position (400, 600 and 800 Hz)
Y1	0.06	0.0501
Y2	0.08	0.0529
Y3	0.11	0.0567
Y4	0.15	0.0671
Y5	0.2	0.0911
Y6	0.24	0.1280
Y7	0.27	0.1632
Y8	0.29	0.2485

mesh and performed the multi-frequency optimization. In the present study, three-frequency optimization was carried out using the same mesh which was used for single-frequency optimization. Due to the inherent advantages of IGA, there was no mesh corruption. The obtained optimal design boundary is shown in Fig. 16(a) and the corresponding reflection spectrum is shown in Fig. 16(b). The obtained shape is very smooth with a low reflection coefficient for all the targeted frequencies. The values of the design variables defining the optimal design boundary are presented in Table 6.

5. Conclusion

The combination of IGA and TLBO has been successfully applied to acoustic horn shape optimization. A Multi-patch model was developed for the acoustic horn which was refined to 150 elements during analysis. The weak form of the acoustic system was solved for pressure distribution and reflection coefficient, R, using IGA. The 8 control points describing the design boundary were considered as the design variables which were modified to reduce the reflection coefficient, R of the horn using the TLBO algorithm. The main advantages of TLBO are: (1) the absence of algorithm-specific tuning parameters unlike other evolutionary optimization algorithms like GA and PSO; (2) no need for gradient computation, unlike gradient-based optimization methods.

In single-frequency optimization, 4 cases (280, 400, 550 and 780 Hz) were considered. The obtained optimal values and the reflection spectra were better than the FEA-based results reported in the literature. IGA-based shape optimization produced better results than FEA-based shape optimization due to the use of higher-order basis functions which increase the analysis accuracy combined with the increased flexibility of the boundary shape deformation through the use of NURBS basis functions. In multi-frequency optimization, two and three-frequency optimization was performed. The obtained optimal shapes were smooth and the reflection spectrum was much better than the FEM-based methods. The three-frequency optimization was performed using the same mesh that was used in single-frequency optimization, unlike earlier methods that used a much finer mesh to avoid mesh corruption leading to convergence issues.

The use of IGA benefited from increased accuracy per degree of freedom, geometry exactness, and convenient refinement which are missing in conventional FEM. The developed platform is readily expandable to optimize 3D problems. However, a considerable increase in computational cost and optimization time is expected. Some of the limitations of the proposed approach are: (1) The possibility of the multiple optimum solutions makes identifying the best solution possible difficult, (2) Increasing the number of design variables leads to wiggly optimum shapes which are not easy to manufacture. In the

future, we are planning to implement the proposed method to optimize other devices relying on acoustic wave propagation and compare the results with those obtained using IGA-BEM.

Declaration of competing interest

The authors declare that they have no known competing financial interests or personal relationships that could have appeared to influence the work reported in this paper.

Appendix A. The patch wise list of control points along with knot vectors of the initial coarse mesh

Patch 1:

Knot vector, u	Knot vector, v	X-Coordinate of the control point	Y-Coordinate of the control point	The weight of the control point
[0, 0, 1, 1]	[0, 0, 0, 0.5, 0.5, 1, 1, 1]	0.1950	0.9807	1
		−0.0248	0.3433	1
		−0.2402	1.0601	0.9137
		−0.1498	0.2808	1
		−0.5975	0.8018	1
		−0.2748	0.2183	1
		−0.9541	0.5361	0.9137
		−0.3998	0.1558	1
		−0.9956	0.0933	1
		−0.5248	0.0933	1

Patch 2:

Knot vector, u	Knot vector, v	X-Coordinate of the control point	Y-Coordinate of the control point	The weight of the control point
[0, 0, 1, 1]	[0, 0, 0, 1, 1, 1]	0.8314	0.5555	1
		0.0000	0.3000	1
		0.6001	0.9000	0.9238
		−0.0124	0.3216	1
		0.1950	0.9807	1
		−0.0248	0.3433	1

Patch 3:

Knot vector, u	Knot vector, v	X-Coordinate of the control point	Y-Coordinate of the control point	The weight of the control point
[0, 0, 0, 1, 1, 1]	[0, 0, 1, 1]	0.0000	0.0000	1
		0.0000	0.1500	1
		0.0000	0.3000	1
		1.0000	0.0000	1
		1.0000	0.2902	0.9569
		0.8314	0.5555	1

Patch 4:

Knot vector, u	Knot vector, v	X-Coordinate of the control point	Y-Coordinate of the control point	The weight of the control point
[0, 0, 0, 1, 1, 1]	[0, 0, 1, 1]	−0.5000	0.0000	1
		−0.5000	0.0250	1
		−0.5000	0.0500	1
		0.0000	0.0000	1
		0.0000	0.1500	1
		0.0000	0.3000	1

Patch 5:

Knot vector, u	Knot vector, v	X-Coordinate of the control point	Y-Coordinate of the control point	The weight of the control point
[0, 0, 1, 1]	[0, 0, 0, 1, 1, 1]	−0.9987	0.0500	1
		−0.5000	0.0500	1
		−0.9996	0.0250	1
		−0.5000	0.0250	1
		−1.0000	−0.0000	1
		−0.5000	0.0000	1

References

Azegami, H., Takeuchi, K., 2006. A smoothing method for shape optimization: traction method using the Robin condition. Int. J. Comput. Methods 3 (01), 21–33.

Bandara, K., Cirak, F., 2018. Isogeometric shape optimisation of shell structures using multi-resolution subdivision surfaces. Comput. Aided Des. 95, 62–71.

Bängtsson, E., Noreland, D., Berggren, M., 2003. Shape optimization of an acoustic horn. Comput. Methods Appl. Mech. Eng. 192 (11–12), 1533–1571.

Barbieri, R., Barbieri, N., 2013. Acoustic horns optimization using finite elements and genetic algorithm. Appl. Acoust. 74 (3), 356–363.

Barbieri, R., Barbieri, N., De Lima, K.F., 2015. Some applications of the PSO for optimization of acoustic filters. Appl. Acoust. 89, 62–70.

Benzaken, J., Herrema, A.J., Hsu, M.C., Evans, J.A., 2017. A rapid and efficient isogeometric design space exploration framework with application to structural mechanics. Comput. Methods Appl. Mech. Eng. 316, 1215–1256.

Bletzinger, K.U., Firl, M., Linhard, J., Wüchner, R., 2010. Optimal shapes of mechanically motivated surfaces. Comput. Methods Appl. Mech. Eng. 199 (5–8), 324–333.

Camp, C.V., Farshchin, M., 2014. Design of space trusses using modified teaching–learning-based optimization. Eng. Struct. 62, 87–97.

Chen, L., Liu, C., Zhao, W., Liu, L., 2018. An isogeometric approach of two dimensional acoustic design sensitivity analysis and topology optimization analysis for absorbing material distribution. Comput. Methods Appl. Mech. Eng. 336, 507–532.

Choi, M.J., Cho, S., 2018. Constrained isogeometric design optimization of lattice structures on curved surfaces: computation of design velocity field. Struct. Multidiscip. Optim. 58 (1), 17–34.

Dodgen, G., Khajah, T., 2018. Shape optimization of an acoustic horn using differential evolution and isogeometric analysis. In: IGA2018. USACM (United States Association for Computational Mechanics).

Farhadinia, B., 2012. Structural optimization of an acoustic horn. Appl. Math. Model. 36 (5), 2017–2030.

Firl, M., Wüchner, R., Bletzinger, K.U., 2013. Regularization of shape optimization problems using FE-based parametrization. Struct. Multidiscip. Optim. 47 (4), 507–521.

Gillebaart, E., De Breuker, R., 2016. Low-fidelity 2D isogeometric aeroelastic analysis and optimization method with application to a morphing airfoil. Comput. Methods Appl. Mech. Eng. 305, 512–536.

Ha, S.H., Choi, K.K., Cho, S., 2010. Numerical method for shape optimization using T-spline based isogeometric method. Struct. Multidiscip. Optim. 42 (3), 417–428.

Henwood, D.J., 1993. The boundary-element method and horn design. J. Audio Eng. Soc. 41 (6), 485–496.

Herath, M.T., Natarajan, S., Prusty, B.G., John, N.S., 2015. Isogeometric analysis and genetic algorithm for shape-adaptive composite marine propellers. Comput. Methods Appl. Mech. Eng. 284, 835–860.

Hirschler, T., Bouclier, R., Duval, A., Elguedj, T., Morlier, J., 2019. Isogeometric sizing and shape optimization of thin structures with a solid-shell approach. Struct. Multidiscip. Optim. 59 (3), 767–785.

Hughes, T.J.R., Cottrell, J.A., Bazilevs, Y., 2005. Isogeometric analysis: CAD, finite elements, NURBS, exact geometry and mesh refinement. Comput. Methods Appl. Mech. Eng. 194, 4135–4195. https://doi.org/10.1016/j.cma.2004.10.008.

Kang, P., Youn, S.K., 2016. Isogeometric shape optimization of trimmed shell structures. Struct. Multidiscip. Optim. 53 (4), 825–845.

Khajah, T., Villamizar, V., 2019. Highly accurate acoustic scattering: Isogeometric Analysis coupled with local high order Farfield Expansion ABC. Comput. Methods Appl. Mech. Eng. 349, 477–498.

Khajah, T., Antoine, X., Bordas, S.P.A., 2017. High-frequency acoustic scattering in the isogeometric analysis. In: Proceedings of the 13th International Conference on Mathematical and Numerical Aspects of Wave Propagation (WAVES 2017). http://hdl.handle.net/10993/28982.

Khajah, T., Antoine, X., Bordas, S.P.A., 2018. B-spline FEM for time-harmonic acoustic scattering and propagation. J. Theor. Comput. Acoust. https://doi.org/10.1142/S2591728518500597.

Kiendl, J., Schmidt, R., Wüchner, R., Bletzinger, K.U., 2014. Isogeometric shape optimization of shells using semi-analytical sensitivity analysis and sensitivity weighting. Comput. Methods Appl. Mech. Eng. 274, 148–167.

Kostas, K.V., Ginnis, A.I., Politis, C.G., Kaklis, P.D., 2017. Shape-optimization of 2D hydrofoils using an isogeometric BEM solver. Comput. Aided Des. 82, 79–87.

Le, C., Bruns, T., Tortorelli, D., 2011. A gradient-based, parameter-free approach to shape optimization. Comput. Methods Appl. Mech. Eng. 200 (9–12), 985–996.

Liu, C., Chen, L., Zhao, W., Chen, H., 2017. Shape optimization of sound barrier using an isogeometric fast multipole boundary element method in two dimensions. Eng. Anal. Bound. Elem. 85, 142–157.

Mair, B.A., 1994. Tikhonov regularization for finitely and infinitely smoothing operators. SIAM J. Math. Anal. 25 (1), 135–147.

Manh, N.D., Evgrafov, A., Gersborg, A.R., Gravesen, J., 2011. Isogeometric shape optimization of vibrating membranes. Comput. Methods Appl. Mech. Eng. 200 (13–16), 1343–1353.

Morgans, R.C., Zander, A.C., Hansen, C.H., Murphy, D.J., 2008. EGO shape optimization of horn-loaded loudspeakers. Optim. Eng. 9 (4), 361–374.

Nagy, A.P., Abdalla, M.M., Gürdal, Z., 2010. Isogeometric sizing and shape optimization of beam structures. Comput. Methods Appl. Mech. Eng. 199 (17–20), 1216–1230.

Nagy, A.P., Abdalla, M.M., Gürdal, Z., 2011. Isogeometric design of elastic arches for maximum fundamental frequency. Struct. Multidiscip. Optim. 43 (1), 135–149.

Nguyen, D.M., Evgrafov, A., Gravesen, J., 2012. Isogeometric shape optimization for electromagnetic scattering problems. Prog. Electromagn. Res. 45, 117–146.

Nørtoft, P., Gravesen, J., 2013. Isogeometric shape optimization in fluid mechanics. Struct. Multidiscip. Optim. 48 (5), 909–925.

Peake, M.J., Trevelyan, J., Coates, G., 2013. Extended isogeometric boundary element method (XIBEM) for two-dimensional Helmholtz problems. Comput. Methods Appl. Mech. Eng. 259, 93–102.

Piegl, L., Tiller, W., 2012. The NURBS Book. Springer Science & Business Media.

Qian, X., 2010. Full analytical sensitivities in NURBS based isogeometric shape optimization. Comput. Methods Appl. Mech. Eng. 199 (29–32), 2059–2071.
Qian, X., Sigmund, O., 2011. Isogeometric shape optimization of photonic crystals via coons patches. Comput. Methods Appl. Mech. Eng. 200 (25–28), 2237–2255.
Rao, R.V., 2016. Teaching Learning Based Optimization Algorithm. Springer, Cham.
Rao, R.V., Patel, V., 2013. Multi-objective optimization of heat exchangers using a modified teaching-learning-based optimization algorithm. Appl. Math. Model. 37, 1147–1162. https://doi.org/10.1016/j.apm.2012.03.043.
Rao, R.V., Savsani, V.J., Vakharia, D.P., 2011. Teaching-learning-based optimization: a novel method for constrained mechanical design optimization problems. Comput. Aided Des. 43, 303–315. https://doi.org/10.1016/j.cad.2010.12.015.
Rao, R.V., Savsani, V.J., Vakharia, D.P., 2012. Teaching-learning-based optimization: an optimization method for continuous non-linear large scale problems. Inf. Sci. 183, 1–15. https://doi.org/10.1016/j.ins.2011.08.006.
Schmidt, S., Wadbro, E., Berggren, M., 2016. Large-scale three-dimensional acoustic horn optimization. SIAM J. Sci. Comput. 38 (6), B917–B940.
Simpson, R.N., Scott, M.A., Taus, M., Thomas, D.C., Lian, H., 2014. Acoustic isogeometric boundary element analysis. Comput. Methods Appl. Mech. Eng. 269, 265–290.
Sun, S.H., Yu, T.T., Nguyen, T.T., Atroshchenko, E., Bui, T.Q., 2018. Structural shape optimization by IGABEM and particle swarm optimization algorithm. Eng. Anal. Bound. Elem. 88, 26–40.
Taheri, A.H., Hassani, B., 2014. Simultaneous isogeometrical shape and material design of functionally graded structures for optimal eigenfrequencies. Comput. Methods Appl. Mech. Eng. 277, 46–80.
Toğan, V., 2012. Design of planar steel frames using teaching–learning-based optimization. Eng. Struct. 34, 225–232.
Ummidivarapu, V.K., Voruganti, H.K., 2017. Shape optimization of two-dimensional structures using isogeometric analysis. Int. J. Eng. Syst. Model. Simul. 9, 169–176. https://doi.org/10.1504/IJESMS.2017.10005510.
Ummidivarapu, V.K., Voruganti, H.K., 2019. Isogeometric boundary element method for analysis and design optimization—a survey. In: Numerical Heat Transfer and Fluid Flow. Springer, Singapore, pp. 177–182.
Vázquez, R., 2016. A new design for the implementation of isogeometric analysis in Octave and Matlab: GeoPDEs 3.0. Comput. Methods Appl. Mech. Eng. 72, 523–554. https://doi.org/10.1016/j.camwa.2016.05.010.
Videla, J., Anitescu, C., Khajah, T., Bordas, S.P., Atroshchenko, E., 2019. h- and p-adaptivity driven by recovery and residual-based error estimators for PHT-splines applied to time-harmonic acoustics. Comput. Math. Appl. 77 (9), 2369–2395.
Wadbro, E., Udawalpola, R., Berggren, M., 2010. Shape and topology optimization of an acoustic horn–lens combination. J. Comput. Appl. Math. 234 (6), 1781–1787.
Wall, W.A., Frenzel, M.A., Cyron, C., 2008. Isogeometric structural shape optimization. Comput. Methods Appl. Mech. Eng. 197, 2976–2988. https://doi.org/10.1016/j.cma.2008.01.025.
Wang, Z.P., Abdalla, M., Turteltaub, S., 2017. Normalization approaches for the descent search direction in isogeometric shape optimization. Comput. Aided Des. 82, 68–78.
Wang, C., Xia, S., Wang, X., Qian, X., 2018a. Isogeometric shape optimization on triangulations. Comput. Methods Appl. Mech. Eng. 331, 585–622.
Wang, Y., Wang, Z.P., Xia, Z., Poh, L.H., 2018b. Structural design optimization using isogeometric analysis: a comprehensive review. Comput. Model. Eng. Sci. 109 (3), 455–507.
Wang, C., Yu, T., Curiel-Sosa, J.L., Xie, N., Bui, T.Q., 2019a. Adaptive chaotic particle swarm algorithm for isogeometric multi-objective size optimization of FG plates. Struct. Multidiscip. Optim., 1–22.
Wang, C., Yu, T., Shao, G., Nguyen, T.T., Bui, T.Q., 2019b. Shape optimization of structures with cutouts by an efficient approach based on XIGA and chaotic particle swarm optimization. Eur. J. Mech. A, Solids 74, 176–187.
Xu, G., Li, B., Shu, L., Chen, L., Xu, J., Khajah, T., 2019. Efficient r-adaptive isogeometric analysis with Winslow's mapping and monitor function approach. J. Comput. Appl. Math. 351, 186–197.
Yoon, M., Ha, S.H., Cho, S., 2013. Isogeometric shape design optimization of heat conduction problems. Int. J. Heat Mass Transf. 62, 272–285.